

Distinct Adsorption Configurations and Self-Assembly Characteristics of Fibrinogen on Chemically Uniform and Alternating Surfaces including Block Copolymer Nanodomains

Sheng Song, Kristina Ravensbergen, Anginelle Alabanza, Danielle Soldin, and Jong-in Hahn*

Department of Chemistry, Georgetown University, 37th & O Streets NW, Washington, D.C. 20057, United States

ABSTRACT Understanding protein–surface interactions is crucial to solid-state biomedical applications whose functionality is directly correlated with the precise control of the adsorption configuration, surface packing, loading density, and bioactivity of protein molecules. Because of the small dimensions and highly amphiphilic nature of proteins, investigation of protein adsorption performed on nanoscale topology can shed light on subprotein-level interaction preferences. In this study, we examine the adsorption and assembly behavior of a highly elongated protein, fibrinogen, on both chemically uniform (as-is and buffered HF-treated SiO₂/Si, and homopolymers of polystyrene and poly(methyl methacrylate)) and varying (polystyrene-*block*-poly(methyl methacrylate)) surfaces. By focusing on high-resolution imaging of individual protein molecules whose configurations are influenced by protein–surface rather than protein–protein interactions, fibrinogen

conformations characteristic to each surface are identified and statistically analyzed for structural similarities/differences in key protein domains. By exploiting block copolymer nanodomains whose repeat distance is commensurate with the length of the individual protein, we determine that fibrinogen exhibits a more neutral tendency for interaction with both polystyrene and poly(methyl methacrylate) blocks relative to the case of common globular proteins. Factors affecting fibrinogen–polymer interactions are discussed in terms of hydrophobic and electrostatic interactions. In addition, assembly and packing attributes of fibrinogen are determined at different loading conditions. Primary orientations of fibrinogen and its rearrangements with respect to the underlying diblock nanodomains associated with different surface coverage are explained by pertinent protein interaction mechanisms. On the basis of two-dimensional stacking behavior, a protein assembly model is proposed for the formation of an extended fibrinogen network on the diblock copolymer.

Surface	AFM of Fg	Schematic of Fg
n-SiO ₂		
m-SiO ₂		
PS		
PMMA		
PS- <i>b</i> -PMMA		

KEYWORDS: fibrinogen · protein adsorption · protein self-assembly · protein surface conformation · protein nanoarray · protein–polymer interaction

Human fibrinogen (Fg) is a protein with a highly elongated shape and composed of three interweaved polypeptide chains of A α , B β , and γ that are connected together by 29 disulfide bonds. The structures of the 340 kDa dimeric protein were first imaged by electron microscopy (EM), revealing the molecular length of 47.5 nm with roughly spherical D and E domains.¹ Later, more complex depictions of Fg such as 45 nm-long heptanodular and octanodular models were reported on the basis of EM and crystallographic observations.^{2–6} In more recent years, atomic force microscopy (AFM) operated in air/liquid has been extensively used to visualize directly Fg in less invasive

sampling conditions involving a biological buffer with no need of staining, crystallization, or vacuum drying.^{7–24} The use of surface-sensitive AFM techniques has been demonstrated for structural investigations of Fg adsorbed on surfaces such as mica, highly oriented pyrolytic graphite, gold, and glass.^{10–21} In some of those cases, original substrates have been further treated with modifying layers such as silane, poly-L-lysine, and self-assembled monolayer compounds before Fg adsorption.^{7–9,13,18} AFM has also been extensively employed to obtain force–distance relationships of Fg interacting with various surfaces.^{22–24} In this paper, we focus our discussions on high-resolution structural investigations of surface-bound Fg using AFM.

* Address correspondence to
jh583@georgetown.edu.

Received for review March 7, 2014
and accepted April 7, 2014.

Published online April 07, 2014
10.1021/nn5013397

© 2014 American Chemical Society

Although variations in the protein length, width, and height are reported depending on the underlying substrates and sampling conditions, a trinodular Fg configuration is predominantly reported in the aforementioned AFM studies. In contrast, the more complex Fg conformations previously reported as the hepta^{2,3} and octanodular⁶ models have rarely been identified *via* AFM, and therefore, their topographic profiles have not been systematically examined in previous AFM studies. Protein imaging parameters such as the size of AFM scan, the surface loading degree of Fg, and the choice of substrates for Fg adsorption can affect the successful identification of topographic details on the single protein and subprotein level. High-resolution structural imaging can be valuable in identifying new protein configurations and protein–surface interaction preferences. Therefore, more AFM efforts with the parameters optimized for imaging individual proteins are warranted to resolve fine topographic features within a single protein. In addition, statistical analyses of the resolved features are needed for the meaningful comparison and correlation of newly observed protein configurations *via* AFM with the chemical/physical properties of the substrates.

One of the major biomedical significances of Fg pertains to its role in thrombosis and how it affects blood coagulation and adhesion of platelets to biomaterial surfaces.²⁵ Polymers are increasingly employed as promising alternatives to existing metallic and ceramic biomaterials as they offer a wide variety of chemical structures and properties.^{26–28} In addition, the application of polymers as coating layers of existing biomaterials has been steadily growing to improve the biocompatibility of metals and ceramics.^{26–28} As such, Fg adsorption studies on polymers whose surfaces are seldom explored in previous AFM investigations of the plasma protein may be highly beneficial to the field of polymer-based biomaterial design and development.

Herein, we carry out topographical examinations to identify surface-dependent Fg conformations at the single protein and subprotein level. Our efforts in this paper focus on high-resolution structural investigations of individual Fg molecules whose configurations are influenced by protein–surface interactions rather than protein–protein interactions in most cases. We then obtain statistical data on Fg subdomain dimensions on both chemically uniform and alternating surfaces. On the basis of high-resolution AFM imaging, we describe in detail the dominant configurations of Fg molecules on five different surfaces that are silicon- and polymer-based. We then compare the preferred protein conformations on each surface on the basis of protein–surface interaction mechanisms. Native oxide-terminated silicon (n-SiO₂, n denoting for the native oxide) and buffered HF-treated silicon (m-SiO₂, m denoting for the modified oxide layer) are

employed as atomically flat surfaces that provide chemically uniform environments for Fg. In addition, two types of widely employed biosubstrates, polystyrene (PS) and poly(methyl methacrylate) (PMMA), are used for Fg adsorption onto chemically uniform, polymeric platforms. Upon surface adsorption, Fg displays distinctively different configurations on these substrates and the subdomain profiles of the protein are systematically catalogued. Observed protein conformations are then discussed with regard to the trinodular and complex models of Fg taken from the EM and crystallographic results.^{1–3,22–24}

A diblock copolymer of polystyrene-*block*-poly(methyl methacrylate) (PS-*b*-PMMA) is chosen as a chemically alternating surface model. We exploit the unique physical and chemical properties of PS-*b*-PMMA nanodomains offering self-assembled, periodically repeating, chemical heterogeneity on the surface.^{29–32} We resolve novel Fg adsorption and assembly behavior on the chemically alternating polymeric domains that specifically present a length scale commensurate with the size of a single Fg. We determine that Fg on PS-*b*-PMMA favors configurations similar to the hepta/octanodular models. In addition, we identify specific adsorption preferences between different subdomains within individual Fg molecules and particular polymeric blocks. The significance of our efforts lies in providing insight to preferential interactions between key Fg domains/chains to specific polymeric nanodomains that has never been observed before. We demonstrate that Fg adsorption behavior onto the PS-*b*-PMMA nanodomains is fairly different from the adsorption behavior of common globular proteins such as immunoglobulin G and bovine serum albumin that were reported earlier on the same polymeric surface.^{33–41} Instead of exhibiting strongly biased and complete segregation to the PS block of PS-*b*-PMMA as seen for the globular proteins,^{33–41} Fg displays adsorption events more neutral to both blocks, involving not only PS but also PMMA phases at specific conditions. We also investigate Fg assembly and orientation into large networks using intermediate and high protein concentration regimes tuned for mono- and multilayer forming conditions on PS-*b*-PMMA. We then elucidate the preferred surface packing configurations and the molecular orientation of Fg with respect to the polymer nanodomain axis under intermediate to high loading conditions.

RESULTS AND DISCUSSION

AFM data presented in Figure 1A–D display substrate-dependent, conformational variations of Fg upon adsorption onto the chemically uniform surfaces of n-SiO₂ (Figure 1A), m-SiO₂ (Figure 1B), PS (Figure 1C), and PMMA (Figure 1D). A total of 20 μg/mL Fg is used for 3 min deposition onto the two silicon-based

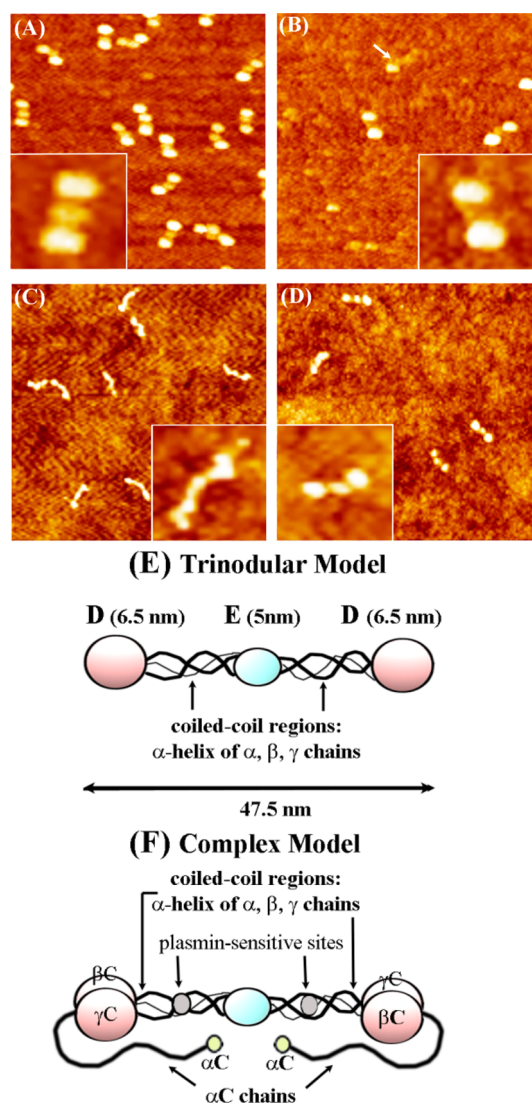


Figure 1. Topographic AFM panels ($500 \text{ nm} \times 500 \text{ nm}$) clearly displaying different morphologies of adsorbed Fg on the chemically uniform surface of (A) n-SiO₂, (B) m-SiO₂, (C) PS homopolymer, and (D) PMMA homopolymer. Insets show a $90 \text{ nm} \times 90 \text{ nm}$ view of an individual Fg molecule on each surface. (E and F) Schematic drawings showing the structure of Fg based on (E) the trinodular model and (F) a more complex model.

surfaces, whereas $5 \mu\text{g/mL}$ of Fg is deposited for 5 min on the two homopolymer-based surfaces. Figure 1E,F shows schematic representations of Fg based on what have been reported earlier in the literature.^{1,6,42} The two commonly discussed Fg models are depicted as the trinodular model in Figure 1E and the complex model in Figure 1F. In the trinodular model portrayed in Figure 1E, Fg consists as three spherical nodules embodying the two D as well as the E domains, and the spherical nodules are linked by coiled-coil connectors.¹ The middle nodule of E is smaller in size than those of D at the ends. The connector cable is reported to be $0.8\text{--}1.5 \text{ nm}$ in diameter and 16 nm in length.¹ In the complex model outlined in Figure 1F, Fg displays heptanodular domains. In this case, each D domain is

divided into two lobes stemming from the independent folding of β and γ chains that are shaped into the βC and γC lobes, respectively.^{2,3,6} A small, non-helical globular domain, serving as a binding site to plasmin, is also included in each coiled-coil arm of the complex model. The α chain is longer than the β and γ chains and extends toward the center of the molecule from the βC and γC lobes, forming a globular αC domain at its C-terminus. Experimental conditions such as pH and certain ion species can affect the degree of the physical separation between the C-termini of the α chains and the E domain *via* the formation of disulfide bonds between the two.⁴²

From all Fg on n-SiO₂ in our AFM measurements, three distinct nodes encompassing the D and E domains are unambiguously observed, see Figure 1A. The overall adsorption configuration resembles the trinodular model rather than the complex model. However, no connector cables are visible in our measurements between the three nodules of Fg on n-SiO₂. This is similar to many previous AFM results reporting similar trinodular Fg shapes on different surfaces.^{9,11,16,19,43} The two models with connector cables in Figure 1E,F are based on EM observations. For EM inspections carried out under vacuum, Fg plates are typically prepared on substrates such as thin carbon films using a high pressure spray gun containing Fg in a volatile buffer mixed with glycerol.^{1,6,42} Subsequently, metal (Pt, Pd, or W) shadowing of the protein is carried out in a vacuum evaporator to increase contrast in electron density. On the other hand, Fg samples for AFM imaging under ambient conditions are usually prepared in physiologically relevant buffers. While these differences in protein sample preparation may result in the morphological disparity involving the connector cable regions observed by AFM and EM, the expected conformations of surface-confined Fg in actual biomaterial applications will mimic what are observed by AFM more closely.

Adsorption onto m-SiO₂ leads to complete unraveling of protein chains for the majority of the surface-bound Fg molecules. Remnants of denatured Fg are frequently observed on m-SiO₂ surface and the typical topographic panels of completely unraveled Fg are provided in Supporting Information, Figure S1. Buffered HF treatment used to prepare m-SiO₂ surface can result in partial fluorination of silicon atoms by forming $(\text{NH}_4)_2\text{SiF}_6$,⁴⁴ and it is well-known that Fg adsorption onto fluorinated polymeric surfaces is greatly discouraged.^{45,46} Our AFM observation of Fg on SiO₂-based surface agrees with these indications of fluorinated surfaces resisting protein adsorption. The number of adsorbed Fg is significantly reduced on m-SiO₂ to approximately 5% of those found on n-SiO₂. For the intact Fg population, only the nodules centering at the D domains are observed on m-SiO₂. The two D nodules of the intact Fg are connected by a thin connecting

thread. In contrast to Fg on $n\text{-SiO}_2$, virtually no node is identified around the E domain, rendering a binodal configuration, Figure 1B. The binodal shape may be an indication of the denaturation process prone to Fg on $m\text{-SiO}_2$. The swollen nodal features of the D domains may be caused by this unraveling of the protein chains. Further chain unfolding may lead to complete denaturing of one or both D domain. The latter is evidenced by a small population of Fg molecules on $m\text{-SiO}_2$ that are intact with only one of the two D domains accompanied by a short tail of thin lines. A typical example of Fg undergoing this chain unraveling process is marked with an arrow in Figure 1B.

Fg on PS homopolymer in Figure 1C reveals a more elongated shape with $13 \pm 0.5\%$ longer than the average length of Fg on PMMA. Fg on PS exhibits a larger number of smaller nodes than what are observed on other chemically uniform surfaces. Both the nodes at the D and E positions are much narrower and thinner in size than those measured on $n\text{-SiO}_2$, $m\text{-SiO}_2$, and PMMA. Connector cables between different nodes are clearly identified from Fg on PS. The elongated conformation and the frequent appearance of small nodes may be attributed to the presence of the αC chains/nodules and plasmin-sensitive sites, similar to what are depicted in the complex model. The typical Fg configuration on the other chemically uniform PMMA surface is shown in Figure 1D. Fg chooses quite different conformations on PMMA when compared to those on PS and the trinodal conformation is observed from the majority of Fg population on PMMA, resembling the protein configuration on SiO_2 . Similar to those on $n\text{-SiO}_2$, no connector threads between the three nodes are observed from Fg on PMMA. However, when comparing the same protein domains between the two surfaces, the spherical nodules around the D and E domains become smaller in size on PMMA than those on SiO_2 . At the same time, the domain size difference between the D and E is larger on $n\text{-SiO}_2$ than that measured between the two domains on PMMA. To recap the preferred conformations of adsorbed Fg on the chemically uniform surfaces, the protein molecules display a binodal configuration on $m\text{-SiO}_2$, a trinodal shape on $n\text{-SiO}_2$ and PMMA, and a more complex configuration on PS. The amount of Fg on the four chemically uniform surfaces is found to be the highest to lowest in the order of $\text{PS} > \text{PMMA} > n\text{-SiO}_2 > m\text{-SiO}_2$.

To elucidate the differences in Fg configurations on polymeric surfaces with nanoscale chemical homogeneity, Fg adsorption characteristics are further investigated on the PS-*b*-PMMA nanodomains. PS-*b*-PMMA diblock copolymer nanodomains form upon thermal annealing above its glass transition temperature in an Ar atmosphere. This phase separation process results in the self-assembly of a chemically alternating, striped surface of PS and PMMA nanodomains whose surface

structures mimic fingerprint patterns. The nanodomains exhibit a repeat spacing of 45 nm while presenting both polymer blocks to the air/polymer interface.^{32,35} This repeat distance is measured along the short axis of the patterns from PS to PS nanodomains (or PMMA to PMMA) and commensurate with the length scale of individual Fg molecules. The persistence length scale of the nanostripes along the long axis of nanodomains is related to the domain curvature which is much larger than the length of a single Fg. A low Fg concentration of 5 $\mu\text{g/mL}$ is deposited for 20 s on PS-*b*-PMMA nanodomains. The highest amount of Fg is found on PS-*b*-PMMA among the five substrates used in this study.

On the periodically repeating polymeric nanotemplates consisting of PS (darker areas in AFM panels) and PMMA (lighter areas) blocks, two orientations are dominantly adopted by Fg as displayed in Figure 2. Adsorption events of the two dominant arrangements on PS-*b*-PMMA are profiled inside the white and black dotted circles in the overlaid topography and phase AFM images of Figure 2A. The first adsorption case groups Fg molecules with the main (D-E-D) axis oriented perpendicular to the long axis of the underlying, striped nanodomains. In this case, the protein adsorption engages both PMMA and PS phases. The second adsorption case yields Fg molecules with the main axis oriented within a single polymeric phase of the PS nanodomain. We define these two Fg adsorption conformations as two phase (*TP*) and single phase (*SP*) orientations. The zoomed-in AFM data in Figure 2B clearly display individual Fg molecules taking the *TP* and *SP* orientations in the left and right panels, respectively. The ratio of the adsorption frequencies between the two orientations is approximately *TP:SP* = 40:60%.

The adsorption characteristics of the elongated Fg, especially in the *TP* orientation, are quite different from what was previously observed from globular proteins on the same types of polymeric surfaces. We and others have previously reported strong adsorption preferences of proteins such as immunoglobulin G (IgG),^{35–38,47,48} bovine serum albumin (BSA),^{35,37,47,48} fibronectin (Fn),³⁷ horseradish peroxidase (HRP),³⁹ mushroom tyrosinase (MT),³⁸ and protein G (PG)³⁵ on the PS block. In the earlier studies carried out by Kumar *et al.* and Lau *et al.*, their adsorption onto PS-*b*-PMMA nanodomains occurs exclusively to the PS domains and the PMMA domains are left completely devoid of the proteins below a monolayer surface coverage.^{35–38,47,48} In contrast to the strongly biased adsorption of the globular proteins, adsorption of Fg on PS-*b*-PMMA tends to be shared by the PS and PMMA blocks.

On the diblock copolymer nanodomains, Fg exhibits an elongated length along its main axis and small multiple nodes on its body, signifying the presence

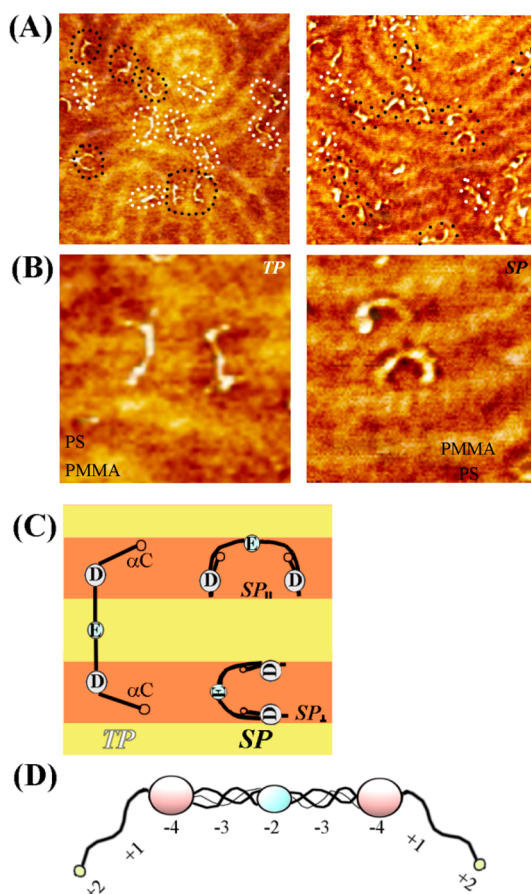


Figure 2. (A) The 500 nm \times 500 nm AFM images display overlaid views of topography and phase scans to show clearly the morphology of adsorbed Fg as well as the underlying PS-*b*-PMMA diblock copolymer nanodomains. In all panels, the lighter (yellow) and darker (orange) domains of the underlying polymeric template are composed of PMMA and PS blocks, respectively. Upon surface adsorption, Fg favors two distinctive orientations of *SP* and *TP*. Individual Fg molecules are grouped into two sets on the basis of their surface adsorption configuration and marked with black and white dotted circles for *SP* and *TP*, respectively. (B) The 160 nm \times 160 nm magnified views of the two dominant orientations of Fg after their adsorption onto PS-*b*-PMMA. Typical examples of *TP* and *SP* adsorption cases are presented in the left and right panel, respectively. (C) Fg configurations typically observed in the *TP* and *SP* adsorption cases are depicted in the cartoon. For *SP*, the main axis of Fg takes one of the two orientations, either parallel and perpendicular with respect to the long axis of the PS domain. They are further categorized as $SP_{||}$ and SP_{\perp} in the diagram. (D) Net charges of key Fg domains under physiological conditions are shown.

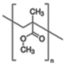
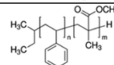
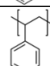
of α C chains. In both *TP* and *SP*, Fg adsorption onto PS-*b*-PMMA nanodomains leads to configurations analogous to the complex model of Figure 1F, yielding results similar to the PS case. In *TP*, the center E domain of Fg lies in the middle of a PMMA domain, positioning the protein main axis vertical to the polymer nanodomain direction. The two D domains at the protein ends are found in the neighboring PS domains. In this adsorption geometry, α C chains are kept spread apart from the center E domain rather than folding toward it. The C-termini of the α chains are placed near the

PMMA domains closest to either end of the protein. In *SP*, the center E domain is located at an interfacial region of PS:PMMA, instead of the middle of a PMMA domain as found in the *TP* case. In *SP*, the protein adapts a bow-shaped curvature while keeping a large section of the Fg main body aligned along the long axis of the underlying nanodomain at the PS:PMMA interface. At the same time, a portion or the entire α C chain folds back toward the protein center in *SP*, instead of spreading away from the main axis of the protein as in *TP*. This folding of α C chain proteins on both ends in *SP* leads to fuller topographic profiles along the main body of Fg than in the *TP* case. The bent configurations of Fg in both *TP* (the bend at the α C chains/domains) and *SP* (the bow-shaped curvature) are similar to EM and X-ray results in that the subdomains of Fg are not located collinearly and a small bend near the two distal end domains gives a better fit than the collinear model in simulating those experimental data.³

It is not yet clear what factors control the *TP* and *SP* orientations of Fg upon adsorption onto PS-*b*-PMMA. When the protein deposition conditions such as the pH, concentration, and the presence of ions are kept the same in our experimental conditions, factors related to the underlying polymeric templates may dictate the occurrence likelihood of the two orientations rather than those associated with proteins. Fg with the *TP* orientation tends to appear more on the nanostripe areas of high curvatures as shown in the left panel of Figure 2A, whereas the *SP* orientation in the right panel of Figure 2A is preferred by regions with straighter nanodomains. In addition, we observe that the *SP* orientation is favored as the protein concentration is increased. The concentration-dependent adsorption behavior will be discussed later in detail with regard to self-assembly of Fg molecules into a large network.

All our AFM data presented in this paper were collected in ambient conditions after gentle N₂ drying of the proteins. AFM imaged in air, the configurations and conformations of the proteins observed in this study will closely mimic the conditions of proteins spotted onto polymeric surfaces of protein microarrays/chips and the environments of proteins linked to silicon-based surfaces in lab-on-a-chip protein detection devices. Therefore, our efforts can be beneficial in developing next-generation nanoprotein arrays and solid-state protein detection devices while providing fundamental insight onto nanoscale adsorption behavior of proteins. It is not clear how proteins adsorb from the solution phase to the surface phase of different polymeric blocks. In buffer, proteins will expose more of their hydrophilic regions to the exterior while burying hydrophobic cores inside. Hence, the initial adsorption of proteins onto PS-*b*-PMMA is likely to be on the PMMA domains followed by migration to PS. This migration may happen sometime after the

TABLE 1. Water Contact Angle and Surface Roughness Values of the Five Substrates Assessed for Fg Adsorption^a

Surface		Chemical Structure	Isoelectric Point pI	H ₂ O contact angle via $\theta/2$ method	Roughness (nm)	
					<i>Ra</i>	<i>Rq</i>
Silicon-based surface	n-SiO ₂	SiO ₂ /Si ^(a)	3.9 ⁵⁴	29°	0.09	0.11
	m-SiO ₂	(NH ₄) ₂ SiF ₆ /Si ^(b)	5.8 ^{54, c)}	58°	0.13	0.16
Polymer-based surface	PMMA		2-4 ⁵⁵	70°	0.30	0.38
	PS- <i>b</i> -PMMA		-	85°	0.32	0.39
	PS		3.5-5 ⁵⁶	92°	0.23	0.29

^a *R_a* and *R_q* correspond to the average roughness and root mean square average roughness, respectively. (a) A network of thin SiO₂ is formed natively on top of a Si wafer. (b) Buffered HF disrupts the extended network of tetrahedral Si(-O)₄ network in the SiO₂ layer and forms (NH₄)₂SiF₆.⁴⁴ (c) The pI value is from a direct HF treatment⁵⁴ (dipped into a 1:50 HF/deionized water (DI) solution for 15 s followed by a 1 min DI rinse) instead of a buffered HF etch.

initial adsorption while still in buffer or during the drying process. When considering the typical translational diffusion coefficient of Fg 2×10^{-7} cm²/s (in water at 37 °C),⁴⁹ Fg can move the characteristic repeat distance of the underlying PS-*b*-PMMA domains (45 nm) approximately in 20 ms. Although the time scale of Fg adsorption onto the polymeric surfaces is determined to be relatively fast in our experiments as several tens of seconds to several minutes, the diffusion-based time scale provides enough opportunities for Fg to adsorb and migrate to the nearby polymeric nanodomains of more preferred interactions after protein chain unfolding. Work to elucidate the extended process of solution to surface adsorption and rates of Fg adsorption/desorption is currently under progress.

Driving forces such as van der Waals (dispersion), electrostatic, hydrogen bonding, and hydrophobic/hydrophilic interactions can affect protein adsorption onto surfaces.^{50–53} Table 1 lists water contact angle values for the five substrates used for Fg adsorption to compare their hydrophobicity characteristics. We have previously reported the important role of hydrophobic/hydrophilic interactions in various adsorption cases of globular proteins onto polymeric surfaces by carrying out control experiments to rule out the effect of the other forces.^{37,41} Similar to the case of globular proteins, hydrophobicity of the underlying substrate seems to play an important role in the adsorption of the highly anisotropically shaped Fg. In our combined AFM and contact angle analysis, Fg conformations analogous to the trinodular and complex model are expected on surfaces with lower and higher hydrophobicity, respectively. This tendency agrees with the general trend for Fg conformations reported previously in different hydrophobic and hydrophilic systems.^{9,15,43} For example, when H₂SO₄/H₂O₂-treated SiO₂ and muscovite mica were used as substrates, trinodular Fg conformations similar to what we have

observed on n-SiO₂ and PMMA were detected.^{9,43} On the other hand, on a titanium oxide surface with a water contact angle of greater than 85°, a more complex morphology of Fg similar to what we have identified on PS and on PS-*b*-PMMA was reported.¹⁵

From the adsorption results gathered in the *TP* case, interaction preferences of each protein subdomain in a single Fg molecule can be deduced with respect to the hydrophobicity/philicity of the two polymeric blocks in PS-*b*-PMMA. Two factors in the *TP* arrangement permit the direct correlation of interaction preferences between the protein subdomains and the polymeric blocks in PS-*b*-PMMA. The first is contributed by the nanoscale diblock copolymer template with chemical heterogeneity on the size scale comparable to the protein length. The second factor is attributed to the fully elongated α C-D-E-D- α C conformation of Fg in *TP* with minimized folding or collapsing of protein chains onto themselves. This unique configuration enables an unambiguous identification of each protein subdomain and its position with respect to PS and PMMA. Our AFM results of Fg in *TP* indicate that E domains favor the hydrophilic PMMA, whereas D domains prefer the more hydrophobic PS. They also suggest that the plasmin-sensitive domains prefer the amphiphilic interfacial areas defined by PS:PMMA and the bulk of the α C chains favors the PS block whereas the α C domains show a preference to PMMA.

The isoelectric points of PS and PMMA are 3.5–5 and 2–4, respectively.^{55,56} At the Fg adsorption condition of pH 7.4, both polymer surfaces have negative charges. PMMA blocks will exhibit more negative character than PS blocks due to the lower pI values. The net charges of each protein subdomain under this pH condition are provided in Figure 2D. The experimental observations made in the *TP* case of Fg can be reasoned from the electrostatic interaction point of view. When considering the D and E domains of Fg, PMMA blocks will be preferred by the E domains as

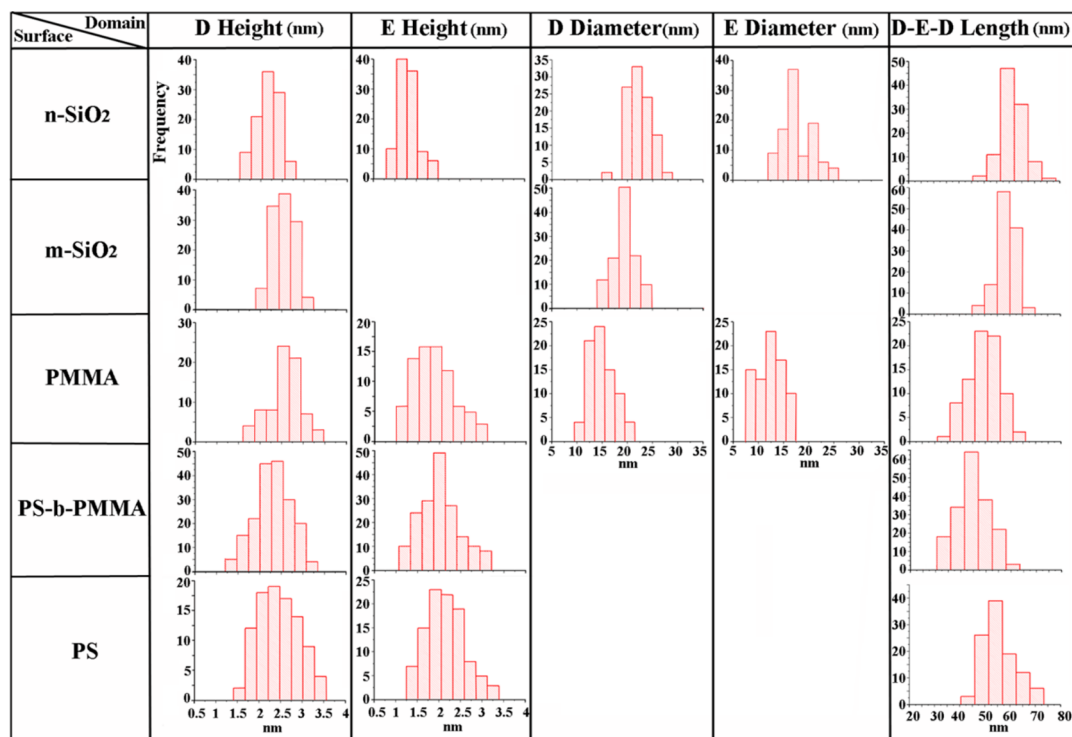


Figure 3. Summarized histogram results for the height, diameter, and length of the D and E domains of Fg on the five substrates. Approximately 100 individual Fg molecules are analyzed on each surface in order to obtain the histograms. The α C chains are not included in the length analysis.

they exhibit a less net negative charge (-2 for the E domain versus -4 for the D domain). Between the α C chains and the main body of Fg, the negatively charged PS domain will tolerate α C chains displaying net positive charges more than the negatively charged main body of the protein. These tendencies agree with the protein configuration in *TP* where the E domain lies in the middle of PMMA, while the α C arms are located in PS. The bow shaped Fg configuration in *SP* may be also reasoned from electrostatic interactions. When α C chains are folded onto the main body of the protein as in the *SP* arrangement, the overlapping of protein chains will lead to partial cancellation of the net negative charges of the Fg main body by the net positive charges of the α C chains. Specifically, the net negative charges on the D domain (-4) and the coiled-coil region (-3) will be offset mainly by the net positive charge of the α C chain ($+1$). On the other hand, the E domain can cancel out their charges more effectively than the D domain *via* its domain-overlapping with the C-terminus of the α C chain (-2 and $+2$, respectively). In this case, the amphiphilic PS:PMMA interfacial regions may be able to attract the charge-neutralized Fg domains effectively. The characteristic shape of Fg molecules commonly observed in the *SP* configuration may stem from the Fg adsorption preference onto the PS:PMMA interfacial regions.

The surface-dependent morphological variations of Fg are catalogued by performing statistical AFM line analysis of the key domains on approximately 100

individual Fg molecules adsorbed on each surface. The average surface roughness values of the underlying substrates measured before protein deposition are provided in Table 1. The AFM roughness measurements indicate that silicon-based surfaces (roughness less than 2 \AA) are slightly smoother than the polymeric platforms ($2\text{--}4 \text{ \AA}$). Figure 3 displays the protein height and diameter histograms of the D and E domains as well as the histograms for the D-E-D domain length. The average values of the key Fg domains are summarized along with their standard deviations in Figure 4. The reported D-E-D length in Figures 3 and 4 does not include that of α C chains. The height of the D domain is found to be the highest on m-SiO₂ whereas the diameters of both the D and E domains are the largest on n-SiO₂. Between polymeric surfaces, the heights of the D and E domains are measured to be similar to one another when comparing the topological profiles of the same Fg domains. When not including α C chains, the protein length is longer on the silicon-based surfaces than on polymeric surfaces. However, when the full length of Fg is considered including the extended α C chains, the most elongated conformation of Fg is found on PS and the second longest on PS-*b*-PMMA. As discussed earlier regarding hydrophobic protein interaction mechanisms, the statistical length data in Figures 3 and 4 indicate that the more elongated Fg configurations are expected on polymeric surfaces with a greater hydrophobic character. A body of earlier work by Wertz *et al.*

Domain	D-h	E-h	D-d	E-d	D-E-D-l	Characteristic domain profile of Fg (side view)
	(nm)	(nm)	(nm)	(nm)	(nm)	
Surface						
n-SiO ₂	2.18 ±0.26	1.31 ±0.22	21.82 ±2.91	17.41 ±3.24	60.86 ±4.74	
m-SiO ₂	2.65 ±0.38	-	19.27 ±2.54	-	57.76 ±3.93	
PMMA	2.58 ±0.56	1.84 ±0.43	14.85 ±2.65	12.35 ±2.59	49.11 ±6.08	
PS- <i>b</i> -PMMA	2.26 ±0.51	2.04 ±0.48	-	-	44.97 ±7.23	
PS	2.52 ±0.62	2.14 ±0.50	-	-	55.57 ±6.74	

Figure 4. Summary of the AFM line analysis based on the Fg adsorption behavior on the five surfaces. D-h, E-h, D-d, E-d, and D-E-D-l denote the height of the D domain, the height of the E domain, the diameter of the D domain, the diameter of the E domain, and the length spanning the D-E-D domains, respectively. The length of the α C domains is not included in the reported D-E-D-l values. The last column provides cartoons of Fg molecules on each surface portraying the characteristic topological features identified by AFM.

has reported extended Fg footprint on a hydrophobic than hydrophilic surface.^{57–59} When bovine Fg adsorption was studied in these efforts *via* total internal reflectance fluorescence on OH- and C16-surfaces with their respective contact angle values of 54–56° and 109–111°, it was also found that Fg footprint was larger on the more hydrophobic surface.^{57–59} While these studies provide valuable insights into the adsorption behavior Fg molecules as an ensemble on hydrophobic *versus* hydrophilic surfaces, our AFM results compliment these earlier work from the adsorption perspective of individual Fg molecules on nanoscale surfaces.

In addition to Fg adsorption at the concentration yielding a low protein number density on the surface of PS-*b*-PMMA as seen in Figure 2, surface assembly characteristics of the protein in intermediate and high concentration regimes are also examined. Under the deposition condition of 20 s with an intermediate concentration of 20 μ g/mL, *SP* arrangements of Fg dominate the adsorption events on PS-*b*-PMMA as displayed in Figure 5. The majority of the protein molecules under this condition is confined to the PS regions of PS-*b*-PMMA, and *TP* adsorption events involving both PMMA and PS domains are significantly reduced. Fg molecules in the *SP* case can exhibit either a perpendicular (SP_{\perp}) or parallel (SP_{\parallel}) orientation on the PS phase with respect to the long axis of the polymeric nanodomains. Typical Fg configurations observed from the two cases of SP_{\perp} and SP_{\parallel} are depicted in the

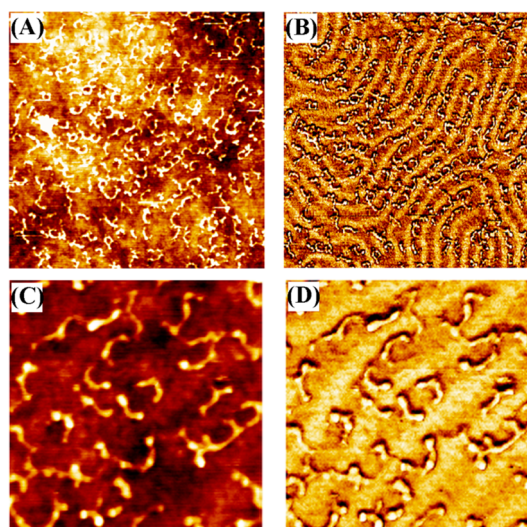


Figure 5. Adsorption behavior of Fg molecules observed on PS-*b*-PMMA nanodomains at an intermediate protein concentration of 20 μ g/mL. (A and B) The 1 μ m \times 1 μ m AFM topography and phase images are displayed in panels A and B, respectively. (C and D) The 200 nm \times 200 nm topography and phase channels in panels C and D show the preferred *SP* arrangement of Fg over the *TP* configuration at this concentration.

diagram shown in Figure 2C. The frequency ratio between the *TP*:*SP* adsorption events is 25:75%. The occurrence ratio between the perpendicular and parallel orientations in *SP* is SP_{\perp} : SP_{\parallel} = 20:80%.

When increasing the Fg concentration further to 50 μ g/mL for the same deposition time, the *SP* adsorption event shows the same growing trend over *TP* and the frequency of the perpendicular orientation rises among Fg molecules taking the *SP* configuration. At this concentration, the ratio between *TP*:*SP* changes to 20:80%, while the occurrence ratio between the perpendicular and parallel orientations in *SP* switches to SP_{\perp} : SP_{\parallel} = 35:65%. The exact source of the preferred *SP* adsorption to *TP* under the increased protein concentration still needs to be determined. It is likely that *SP* arrangements may be due to more dominant influence of the hydrophobic interactions between Fg and PS over the electrostatic interactions associated with the net charges of Fg subdomains and the PS and PMMA phases. For systems involving a larger number of proteins, the free energy of the surface-bound proteins can be effectively lowered by driving many protein molecules to the more hydrophobic phase of PS than to PMMA, although such processes may result in electrostatic energy penalties. When taking both the protein and surface into consideration, the electrostatic penalty in *SP* is due to the tendency for α C domains/chains to prefer PMMA to PS. However, from the electrostatic considerations of solely the protein not including the polymeric substrate, Fg assembled in *SP* configuration can minimize the electrostatic repulsions from different protein subdomains more

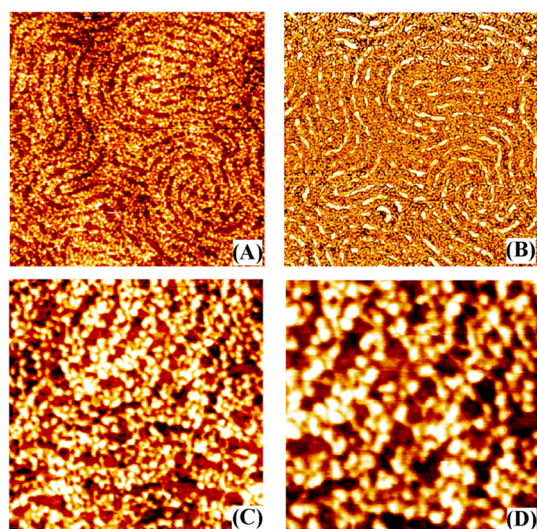


Figure 6. Extended Fg self-assembly into monolayer-forming patterns when depositing $100 \mu\text{g}/\text{mL}$ Fg for 20 s on PS-*b*-PMMA. AFM images of (A) $1 \mu\text{m} \times 1 \mu\text{m}$ topography, (B) $1 \mu\text{m} \times 1 \mu\text{m}$ phase, (C) $400 \text{ nm} \times 400 \text{ nm}$ topography, and (D) $200 \text{ nm} \times 200 \text{ nm}$ topography show the packing configuration of self-arranged Fg which faithfully reproduces the underlying PS-*b*-PMMA nanodomain patterns.

effectively than *TP*. In *SP*, the net negative charges along the main body of Fg are neutralized by the net positive charges of the αC domains placed spatially in close proximity. A more neutralized net charge of Fg can be realized in the αC arm-folded *SP*. When the number of adsorbed proteins increases in PS-*b*-PMMA, this minimization of the electrostatic repulsion between Fg molecules themselves in *SP* may enable dense assembly and packing of Fg molecules close to one another on the surface.

A full surface coverage of Fg on all available PS domains of PS-*b*-PMMA is obtained when the protein concentration is further increased to $100 \mu\text{g}/\text{mL}$. We define this surface loading condition as the monolayer-forming state. Assembled protein patterns under this condition are shown in the topography and phase AFM images in Figure 6 which faithfully reproduce the shape of the underlying polymeric nanodomains. From the physical size of Fg and the available PS area in PS-*b*-PMMA, we determine that this protein deposition condition yields a loading density of $0.94 \text{ mg}/\text{m}^2$. Although it is difficult to discern individual Fg molecules at this surface coverage, several interesting observations are made from the self-assembled network of Fg that are different from the previously reported, monolayer-forming patterns of the globular protein, IgG.^{35,37,41} Two IgG proteins tend to pack side by side along the minor axis of the polymeric nanodomain on PS.³⁵ In contrast, the monolayer patterns of Fg on PS-*b*-PMMA contain lobes that typically appear as triplets along the short axis of the nanodomain. In addition, periodically spaced, thin lines spanning over PMMA domains are identified. The lines connect two

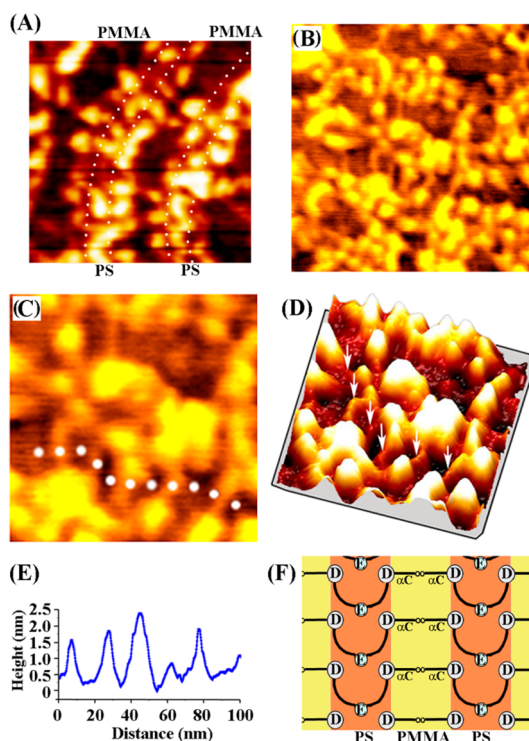


Figure 7. Fg assembly at the monolayer-forming condition. (A) The $90 \text{ nm} \times 90 \text{ nm}$ AFM topographic image displays the appearance of Fg lobes on PS domains in three distinctive strips which run parallel to the long axis of the polymeric nanodomain. The brightness and contrast of the image are modified so that only the lobes on PS domains are visible in the frame. Dashed white lines are added to the image in order to classify the three chains of lobes. (B and C) Linker lines connecting Fg lobes on different PS domains are shown in the 2D topography images with the scan size of (B) $150 \text{ nm} \times 150 \text{ nm}$ and (C) $90 \text{ nm} \times 90 \text{ nm}$. The image contrast is restored to show the topological features on all area of the surface. (D) A $90 \text{ nm} \times 90 \text{ nm}$ 3D topography profile from the same area in the 2D view of panel (C) shows the linker lines on PMMA. To guide the eye, each traversing line on PMMA is highlighted with the inserted white arrow. (E) AFM section analysis along the white dotted line in panel C indicates that the periodicity of the linker lines bridging Fg molecules between two neighboring PS domains is approximately 18.8 nm . (F) A plausible Fg assembly model on PS-*b*-PMMA nanodomains is hypothesized on the basis of the appearance of the triplet lobes and linker lines. The model displays a close-packing geometry of bow-shaped Fg molecules in perpendicular rather than parallel orientation with respect to the long axis of the polymeric nanodomain.

closest Fg lobes, each lying on different PS domains. Such structures that have not been observed before in the globular protein self-assembly are discussed in detail in the following section.

Figure 7A displays a contrast-adjusted topography image to show only the triplet Fg lobes packed on the PS domains. Three distinctive regions of lobes are observed parallel to the long axis of the polymeric nanodomain, forming a chain of Fg lobes in each region. These areas of chained lobes are marked with dashed white lines in Figure 7A. The assembly pattern implies that the close surface packing of the bow-shaped Fg molecules is favored in perpendicular rather

than parallel orientation with respect to the long axis of the PS-*b*-PMMA nanodomain. When the AFM image contrast is restored to show topological features appearing on both polymeric domains, a new topological feature of thin lines traversing over the PMMA domains is clearly visible as displayed in Figure 7B. Fg lobes located on the PS domains on either side of the PMMA are connected *via* these lines. The magnified 2D and 3D images of Figure 7C,D display the periodically appearing linkers. They may be attributed to the α C chains donated from each side by a pair of Fg molecules, each Fg lying on two neighboring PS domains. Packed this way on PS-*b*-PMMA, the free energy of surface-bound Fg may benefit from both standpoints of hydrophobic and electrostatic interactions. The main bodies of packed protein molecules are located on the PS domains for maximizing hydrophobic interactions. In addition, α C chains from each Fg pair are unfolded away from the main body of Fg and placed over the PMMA domains, which is more electrostatically favored than having the α C chains folded on PS. AFM section measurement is performed on the periodic linker lines marked with a white dashed line in Figure 7C and a series of white arrows in Figure 7D. The results in Figure 7E reveal that the linker lines exhibit a repeat spacing of 18.8 nm. The characteristic Fg assembly patterns on PS-*b*-PMMA may be explained by a surface packing model hypothesized in the schematic representation shown in Figure 7F. The suggested model is based on our AFM topographic results exhibiting the typical appearance of triplet lobes along the short axis of the PS nanodomain. The two close-packing scenarios in the parallel and perpendicular orientations of bow-shaped Fg molecules can lead to two and three chains of lobes along the long axis of the polymer nanodomain, respectively. In the assembly model suggested in Figure 7F, the bow-shaped Fg molecules surface-pack on the PS domains *via* the latter scenario and form a stack of bows whose major protein axis is oriented perpendicular to the long axis of the polymeric nanodomain. The linker lines are established between the D domains of Fg on a PS domain and another closely located D domains from a different Fg on a neighboring PS domain.

Figure 8 displays topography panels of surface-bound Fg on the three polymeric surfaces of PS, PMMA, and PS-*b*-PMMA when Fg concentrations of 1000 μ g/mL for PS and PMMA and 500 μ g/mL for PS-*b*-PMMA are used for 20 s deposition. We estimate that the respective Fg deposition conditions lead to the protein surface density of 1.6, 1.2, and 1.8 mg/m² on PS, PMMA, and PS-*b*-PMMA, respectively. Figure 8A,B shows typical topographic panels of Fg adsorbed on PS and PMMA homopolymer, respectively, whereas Figure 8C,D has the adsorption results on the PS-*b*-PMMA nanodomains. The number density of surface-bound proteins is highest to lowest in the order of PS-*b*-PMMA, PS, and

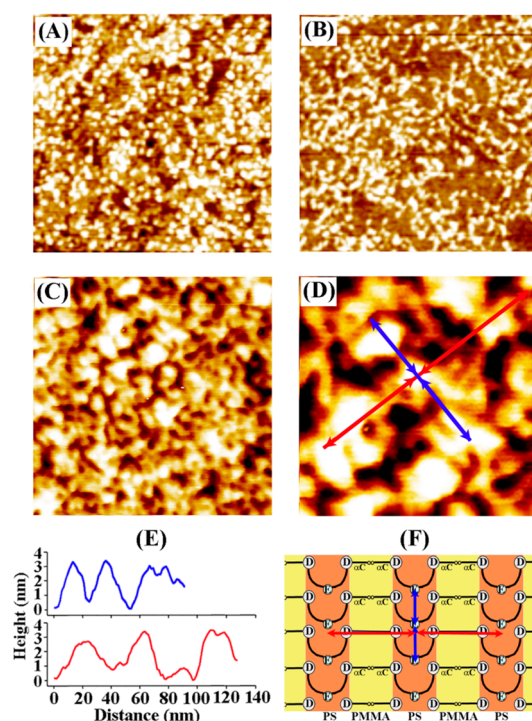


Figure 8. (A and B) Fg adsorption behavior is shown in the 350 nm \times 350 nm AFM topography panels when a higher protein concentration of 1000 μ g/mL is used onto (A) PS and (B) PMMA homopolymer surfaces. (C–F) Fg adsorption morphology on PS-*b*-PMMA is shown in the (C) 180 nm \times 180 nm and (D) 90 nm \times 90 nm AFM topography panels when using a 500 μ g/mL protein solution. (E) Although the underlying stripe patterns of the diblock copolymer nanodomains are no longer clearly visible under these conditions, the height profiles of the assembled Fg display distinctively periodic spacings in two directions. Results from the height analysis along the blue and red lines in panel D are shown. (F) The repeat distances along the red and blue lines are correlated with the intermolecular spacing between relevant protein domains using the same Fg surface assembly model shown in Figure 7F.

PMMA similar to the surface density order reported for the globular protein of IgG.³⁷ Fg forms a dense network on the PS-*b*-PMMA surface and the striped patterns defined by the underlying polymeric nanodomains are no longer clearly identifiable in Figure 8C. Bigger grains and interlacing strings appear on the entire surface at this concentration, instead of the smaller lobes seen in Figure 7. It is likely that the grains are formed by a cluster of layered lobes. As profiled in Figure 8E, AFM line analysis on these grains in the two directions of the blue and red arrows marked in Figure 8D shows a shorter and longer, periodic spacing of 20 and 40 nm, respectively. These repeat distances are correlated with the intermolecular distances of Fg in two orthogonal directions in the assembly model presented in Figure 8F. In this model, the short repeat distance is attributed to the spacing between two Fg molecules adsorbed on the same PS domain, whereas the gap between the periodically arranged Fg molecules on two different PS domains is responsible for the long repeat distance.

CONCLUSION

In summary, we systematically examine surface-specific Fg conformations on silicon-based ($n\text{-SiO}_2$, $m\text{-SiO}_2$) and polymer-based (PS, PMMA, PS-*b*-PMMA) substrates by first performing high-resolution AFM imaging focusing on individual proteins and then by statistically analyzing the topological profiles of key subdomains on each surface. We discuss the differences and similarities between the characteristic adsorption behavior of the highly anisotropically shaped Fg molecule in terms of the physical/chemical properties of the substrate, protein–polymer interaction forces, protein surface density, and trinodular/complex conformational models. We investigate Fg subdomain-specific adsorption preferences and orientations to the PS and PMMA block by exploiting PS-*b*-PMMA diblock copolymer nanodomains, which provide a periodically and chemically varying surface on the length scale commensurate with single Fg molecules. Adsorption behavior of the Fg is compared to that of common globular proteins reported earlier on the

same nanoscale polymeric domains. Adsorption of Fg molecules is affected less by the exclusive interaction between the protein and the PS block and Fg exhibits a more neutral tendency for shared interaction with both PS and PMMA blocks. We also examine Fg configurations and molecular orientations during its assembly and surface packing into a larger protein network. We hypothesize Fg assembly and packing model on PS-*b*-PMMA on the basis of the AFM results, which signifies the first attempt to discern Fg domain-specific interaction preferences to chemically alternating, nanoscale surfaces. In this assembly model, the bow-shaped Fg molecules in *SP* configuration surface-pack on the PS domains by forming a stack of bows whose major protein axis is perpendicular to the long axis of the polymeric nanodomain. The linker lines are established *via* stretched α C chains over PMMA connecting between the D domain of a Fg molecule on a PS domain and a closely located D domain from another Fg molecule situated on a neighboring PS domain.

METHODS

Silicon-based substrates of $n\text{-SiO}_2$ and $m\text{-SiO}_2$ are prepared by using Si wafers (resistivity $< 1 \Omega \text{ cm}$, thickness: 0.017 in.) obtained from Silicon Quest International, Inc. (San Jose, CA). The surface of $n\text{-SiO}_2$ contains a natively formed oxide layer on top of Si and is used as is after cleaning with deionized water (DI) and ethanol. The surface of $m\text{-SiO}_2$ is prepared by immersing the precleaned substrate in a buffered HF etching medium (6:1 volume ratio of 40% NH_4F :49% HF in DI) for 2 min and then rinsing with an ample amount of DI. The substrates are then dried under a gentle stream of N_2 before use. Polymer-based substrates of PS, PMMA, and PS-*b*-PMMA are prepared from the homopolymer and diblock copolymer granules received from Polymer Source, Inc. (Montreal, Canada). The average molecular weight of PS, PMMA, and PS-*b*-PMMA (71% PS by weight) is 152, 120, and 71.4 kDa, respectively, and their polydispersity is 1.06. Both chemically uniform (PS and PMMA homopolymers) and alternating (PS-*b*-PMMA diblock copolymer) surfaces are made by spin coating 2% (w/v) polymeric solutions at 3500 rpm for 1 min on Si, which is precleaned with a series of solvents using ethanol, acetone, and toluene. Phase separation of PS-*b*-PMMA is subsequently achieved *via* thermal annealing in an Ar atmosphere at 240 °C for 6 h with a transient ramp-up rate of 5 K/min and a cooling rate of 2 K/min. This process yields periodically alternating and chemically varying nanodomains which are known as half-cylinders and exposes repeating stripes of PS and PMMA blocks at the air/polymer interface with repeat units of 45 nm (PS to PS distance).^{31,32,35} Fg, human plasma fibrinogen, is purchased from VWR Scientific, Inc. (West Chester, PA). The lyophilized powder of Fg is reconstituted in PBS buffer (10 mM mixture of Na_2HPO_4 and NaH_2PO_4 , 140 mM NaCl, 3 mM KCl, pH 7.4) and diluted to varying concentrations ranging from 5 to 1000 $\mu\text{g/mL}$. A volume of 10–100 μL of Fg solution is applied to the desired substrate and placed in a humidity-controlled chamber for time spans of 20 s to 5 min. The deposition conditions such as protein concentration and incubation time are controlled to vary the surface density of adsorbed proteins from sparsely to densely populated cases, as needed. The sample surfaces are then carefully rinsed with 40 μL of PBS multiple times, followed by a thorough rinsing with DI and a gentle drying under a stream of N_2 before protein characterization. Water contact angles of all substrates are measured using a Tantec contact angle meter (Chemsultants

International, Inc., Fairfield, OH) with a half angle method prior to protein deposition. Surface roughness of the substrates prior to protein deposition and characteristic Fg conformations on different surfaces are profiled and analyzed by performing high-resolution AFM imaging focusing on individual Fg molecules. Topography and phase scans are carried out with a MultiMode 8 AFM interfaced with a Nanoscope V controller (Bruker Corp., Santa Barbara, CA), operated in a soft tapping mode at a scan speed of 1 Hz or lower using silicon tips with a typical resonant frequency of 60–70 kHz and a spring constant of 1–5 N/m. The statistical data for the height, diameter, and length of the key subdomains in Fg are obtained by measuring the topographic profiles of approximately 100 protein molecules on each surface.

Conflict of Interest: The authors declare no competing financial interest.

Acknowledgment. The authors thank Dr. N. Kumar for carrying out preliminary AFM measurements on PS-*b*-PMMA and acknowledge financial support on this work by the National Institutes of Health, National Research Service Award (1R01DK088016) from the National Institute of Diabetes and Digestive and Kidney Diseases.

Supporting Information Available: AFM data showing the completely unraveled Fg on $m\text{-SiO}_2$. This material is available free of charge *via* the Internet at <http://pubs.acs.org>.

REFERENCES AND NOTES

- Hall, C. E.; Slayter, H. S. The Fibrinogen Molecule: Its Size, Shape, and Mode of Polymerization. *J. Biophys. Biochem. Cytol.* **1959**, *5*, 11–27.
- Weisel, J. W.; Phillips, G. N.; Cohen, C. A Model from Electron Microscopy for the Molecular Structure of Fibrinogen and Fibrin. *Nature* **1981**, *289*, 263–267.
- Weisel, J. W.; Stauffacher, C. V.; Bullitt, E.; Cohen, C. A Model for Fibrinogen: Domains and Sequence. *Science* **1985**, *230*, 1388–1391.
- Kollman, J. M.; Pandi, L.; Sawaya, M. R.; Riley, M.; Doolittle, R. F. Crystal Structure of Human Fibrinogen. *Biochemistry* **2009**, *48*, 3877–3886.
- Yang, Z.; Mochalkin, I.; Veerapandian, L.; Riley, M.; Doolittle, R. F. Crystal Structure of Native Chicken Fibrinogen at

- 5.5-Å Resolution. *Proc. Natl. Acad. Sci. U.S.A.* **2000**, *97*, 3907–3912.
6. Hantgan, R. R.; Lord, S. T. Fibrinogen Structure and Physiology. In *Hemostasis and Thrombosis: Basic Principles and Clinical Practice*; Colman, R. W., Marder, V. J., Clowes, A. W., George, J. N., Goldhaber, S. Z., Eds.; Lippincott Williams & Wilkins: Philadelphia, PA, 2006.
 7. Marchant, R. E.; Barb, M. D.; Shainoff, J. R.; Eppell, S. J.; Wilson, D. L.; Siedlecki, C. A. Three Dimensional Structure of Human Fibrinogen under Aqueous Conditions Visualized by Atomic Force Microscopy. *Thromb. Haemostasis* **1997**, *77*, 1048–1051.
 8. Taatjes, D. J.; Quinn, A. S.; Jenny, R. J.; Hale, P.; Bovill, E. G.; McDonagh, J. A. N. Tertiary Structure of the Hepatic Cell Protein Fibrinogen in Fluid Revealed by Atomic Force Microscopy. *Cell Biol. Int.* **1997**, *21*, 715–726.
 9. Sit, P. S.; Marchant, R. E. Surface-Dependent Conformations of Human Fibrinogen Observed by Atomic Force Microscopy under Aqueous Conditions. *Thromb. Haemostasis* **1999**, *82*, 1053–1060.
 10. Wasilewska, M.; Adamczyk, Z. Fibrinogen Adsorption on Mica Studied by AFM and *in Situ* Streaming Potential Measurements. *Langmuir* **2010**, *27*, 686–696.
 11. Ohta, R.; Saito, N.; Ishizaki, T.; Takai, O. Visualization of Human Plasma Fibrinogen Adsorbed on Highly Oriented Pyrolytic Graphite by Scanning Probe Microscopy. *Surf. Sci.* **2006**, *600*, 1674–1678.
 12. Jandt, K. D. Atomic Force Microscopy of Biomaterials Surfaces and Interfaces. *Surf. Sci.* **2001**, *491*, 303–332.
 13. Averetta, L. E.; Schoenfish, M. H. Atomic Force Microscope Studies of Fibrinogen Adsorption. *Analyst* **2010**, *135*, 1201–1209.
 14. Marchin, K. L.; Berrie, C. L. Conformational Changes in the Plasma Protein Fibrinogen upon Adsorption to Graphite and Mica Investigated by Atomic Force Microscopy. *Langmuir* **2003**, *19*, 9883–9888.
 15. Cacciafesta, P.; Humphris, A. D. L.; Jandt, K. D.; Miles, M. J. Human Plasma Fibrinogen Adsorption on Ultraflat Titanium Oxide Surfaces Studied with Atomic Force Microscopy. *Langmuir* **2000**, *16*, 8167–8175.
 16. Tunc, S.; Maitz, M. F.; Steiner, G.; Vázquez, L.; Pham, M. T.; Salzer, R. *In Situ* Conformational Analysis of Fibrinogen Adsorbed on Si Surfaces. *Colloids Surf., B* **2005**, *42*, 219–225.
 17. Ta, T. C.; Sykes, M. T.; McDermott, M. T. Real-Time Observation of Plasma Protein Film Formation on Well-Defined Surfaces with Scanning Force Microscopy. *Langmuir* **1998**, *14*, 2435–2443.
 18. Wigren, R.; Elwing, H.; Erlandsson, R.; Welin, S.; Lundström, I. Structure of Adsorbed Fibrinogen Obtained by Scanning Force Microscopy. *FEBS Lett.* **1991**, *280*, 225–228.
 19. Lin, Y.; Wang, J.; Wan, L.-J.; Fang, X.-H. Study of Fibrinogen Adsorption on Self-Assembled Monolayers on Au(111) by Atomic Force Microscopy. *Ultramicroscopy* **2005**, *105*, 129–136.
 20. Van De Keere, I.; Willaert, R.; Hubin, A.; Vereecken, J. Interaction of Human Plasma Fibrinogen with Commercially Pure Titanium as Studied with Atomic Force Microscopy and X-ray Photoelectron Spectroscopy. *Langmuir* **2008**, *24*, 1844–1852.
 21. Jandt, K. D.; Finke, M.; Cacciafesta, P. Aspects of the Physical Chemistry of Polymers, Biomaterials and Mineralised Tissues Investigated with Atomic Force Microscopy. *Colloids Surf., B* **2000**, *19*, 301–314.
 22. Xu, L.-C.; Siedlecki, C. A. Atomic Force Microscopy Studies of the Initial Interactions between Fibrinogen and Surfaces. *Langmuir* **2009**, *25*, 3675–3681.
 23. Soman, P.; Siedlecki, C. A. Effects of Protein Solution Composition on the Time-Dependent Functional Activity of Fibrinogen on Surfaces. *Langmuir* **2011**, *27*, 10814–10819.
 24. Soman, P.; Rice, Z.; Siedlecki, C. A. Measuring the Time-Dependent Functional Activity of Adsorbed Fibrinogen by Atomic Force Microscopy. *Langmuir* **2008**, *24*, 8801–8806.
 25. Loscalzo, J.; Schafer, A. I. *Thrombosis and Hemorrhage*; Lippincott Williams & Wilkins: Philadelphia, PA, 2003.
 26. Dumitriu, S.; Popa, V. I. *Polymeric Biomaterials*; CRC Press: Boca Raton, FL, 2013.
 27. Ratner, B. D.; Hoffman, A. S.; Schoen, F. J.; Lemons, J. E. *Biomaterials Science: An Introduction to Materials in Medicine*; Elsevier Science: Waltham, MA, 2012.
 28. Keller, T. F.; Schönfelder, J.; Reichert, J.; Tuccitto, N.; Licciardello, A.; Messina, G. M. L.; Marletta, G.; Jandt, K. D. How the Surface Nanostructure of Polyethylene Affects Protein Assembly and Orientation. *ACS Nano* **2011**, *5*, 3120–3131.
 29. Hahm, J.; Lopes, W. A.; Jaeger, H. M.; Sibener, S. J. Defect Evolution in Ultrathin Films of Polystyrene-block-polymethylmethacrylate Diblock Copolymers Observed by Atomic Force Microscopy. *J. Chem. Phys.* **1998**, *109*, 10111–10114.
 30. Hahm, J.; Sibener, S. J. Cylinder Alignment in Annular Structures of Microphase-Separated Polystyrene-*b*-Poly(methyl methacrylate). *Langmuir* **2000**, *16*, 4766–4769.
 31. Hahm, J.; Sibener, S. J. Time-Resolved Atomic Force Microscopy Imaging Studies of Asymmetric PS-*b*-PMMA Ultrathin Films: Dislocation and Disclination Transformations, Defect Mobility, and Evolution of Nanoscale Morphology. *J. Chem. Phys.* **2001**, *114*, 4730–4740.
 32. Morkved, T. L.; Lopes, W. A.; Hahm, J.; Sibener, S. J.; Jaeger, H. M. Silicon Nitride Membrane Substrates for the Investigations of Local Structures in Polymer Thin Films. *Polymer* **1998**, *39*, 3871.
 33. Hahm, J. I. Polymeric Surface-Mediated, High-Density Nano-Assembly of Functional Protein Arrays. *J. Biomed. Nanotechnol.* **2011**, *7*, 731–742.
 34. Hahm, J. I. Functional Polymers in Protein Detection Platforms: Optical, Electrochemical, Electrical, Mass-Sensitive, and Magnetic Biosensors. *Sensors* **2011**, *11*, 3327–3355.
 35. Kumar, N.; Hahm, J. Nanoscale Protein Patterning using Self-Assembled Diblock Copolymers. *Langmuir* **2005**, *21*, 6652–6655.
 36. Kumar, N.; Parajuli, O.; Dorfman, A.; Kipp, D.; Hahm, J. Activity Study of Self-Assembled Proteins on Nanoscale Diblock Copolymer Templates. *Langmuir* **2007**, *23*, 7416–7422.
 37. Kumar, N.; Parajuli, O.; Gupta, A.; Hahm, J. Elucidation of Protein Adsorption Behavior on Polymeric Surfaces: Towards High Density, High Payload, Protein Templates. *Langmuir* **2008**, *24*, 2688–2694.
 38. Kumar, N.; Parajuli, O.; Hahm, J. Two-Dimensionally Self-Arranged Protein Nanoarrays on Diblock Copolymer Templates. *J. Phys. Chem. B* **2007**, *111*, 4581–4587.
 39. Parajuli, O.; Gupta, A.; Kumar, N.; Hahm, J. Evaluation of Enzymatic Activity on Nanoscale PS-*b*-PMMA Diblock Copolymer Domains. *J. Phys. Chem. B* **2007**, *111*, 14022–14027.
 40. Song, S.; Milchak, M.; Zhou, H. B.; Lee, T.; Hanscom, M.; Hahm, J. I. Nanoscale Protein Arrays of Rich Morphologies via Self-Assembly on Chemically Treated Diblock Copolymer Surfaces. *Nanotechnology* **2013**, *24*, 10.
 41. Hahm, J. Fundamentals of Nanoscale Polymer-Protein Interactions and Potential Contributions to Solid-State Nanobioarrays. *Langmuir* **2014**, *30*, 10211/1a404481t.
 42. Veklich, Y. I.; Gorkun, O. V.; Medved, L. V.; Nieuwenhuizen, W.; Weisel, J. W. Carboxyl-Terminal Portions of the α Chains of Fibrinogen and Fibrin. Localization by Electron Microscopy and the Effects of Isolated α C Fragments on Polymerization. *J. Biol. Chem.* **1993**, *268*, 13577–13585.
 43. Toscano, A.; Santore, M. M. Fibrinogen Adsorption on Three Silica-Based Surfaces: Conformation and Kinetics. *Langmuir* **2006**, *22*, 2588–2597.
 44. Kikyuama, H.; Miki, N.; Saka, K.; Takano, J.; Kawanabe, I.; Miyashita, M.; Ohmi, T. Principles of Wet Chemical Etching Process in ULSI Microfabrication. *IEEE Trans. Semicond. Manuf.* **1991**, *4*, 26–35.
 45. Jahangir, A. R.; McClung, W. G.; Cornelius, R. M.; McCloskey, C. B.; Brash, J. L.; Santerre, J. P. Fluorinated Surface-Modifying Macromolecules: Modulating Adhesive Protein and Platelet Interactions on a Polyether-Urethane. *J. Biomed. Mater. Res., Part A* **2002**, *60*, 135–147.
 46. Jannasch, P. Surface Structure and Dynamics of Block and Graft Copolymers having Fluorinated Poly(ethylene oxide) Chain Ends. *Macromolecules* **1998**, *31*, 1341–1347.

47. Lau, K. H. A.; Bang, J.; Hawker, C. J.; Kim, D. H.; Knoll, W. Modulation of Protein-Surface Interactions on Nano-patterned Polymer Films. *Biomacromolecules* **2009**, *10*, 1061–1066.
48. Lau, K. H. A.; Bang, J.; Kim, D. H.; Knoll, W. Self-Assembly of Protein Nanoarrays on Block Copolymer Templates. *Adv. Funct. Mater.* **2008**, *18*, 3148–3157.
49. Martinez, M. C. L.; Rodes, V.; Garcia de la Torre, J. Estimation of the Shape and Size of Fibrinogen in Solution from its Hydrodynamic Properties using Theories for Bead Models and Cylinders. *Int. J. Biol. Macromol.* **1984**, *6*, 261–265.
50. Bamford, C. H.; Cooper, S. L.; Tsuruta, T. *The Vroman Effect*; VSP BV: The Netherlands, 1992.
51. Damme, H. S. V.; Beugeling, T.; Ratering, M. T.; Feijen, J. Protein Adsorption from Plasma onto Poly(n-alkyl) methacrylate Surfaces, In *The Vroman Effect*; Bamford, C. H., Cooper, S. L., Tsurutta, T., Eds.; VSP: Utrecht, The Netherlands, 1992; pp 123–138.
52. Latour, R. A. Biomaterials: Protein–Surface Interactions. In *Encyclopedia of Biomaterials and Biomedical Engineering*, 2nd ed.; Informa Healthcare: New York, 2008; Vol. 1, pp 270–284.
53. Tsapikouni, T. S.; Missirlis, Y. F. pH and Ionic Strength Effect on Single Fibrinogen Molecule Adsorption on Mica Studied with AFM. *Colloids Surf., B* **2007**, *57*, 89–96.
54. Trevino, K. J.; Shearer, J. C.; Tompkins, B. D.; Fisher, E. R. Comparing Isoelectric Point and Surface Composition of Plasma Modified Native and Deposited SiO₂ Films Using Contact Angle Titrations and X-ray Photoelectron Spectroscopy. *Plasma Process. Polym.* **2011**, *8*, 951–964.
55. Beattie, J. K. The Intrinsic Charge on Hydrophobic Microfluidic Substrates. *Lab Chip* **2006**, *6*, 1409–1411.
56. Bolt, P. S.; Goodwin, J. W.; Ottewill, R. H. Studies on the Preparation and Characterization of Monodisperse Polystyrene Latices. VI. Preparation of Zwitterionic Latices. *Langmuir* **2005**, *21*, 9911–9916.
57. Wertz, C. F.; Santore, M. M. Fibrinogen Adsorption on Hydrophilic and Hydrophobic surfaces: Geometrical and Energetic Aspects of Interfacial Relaxations. *Langmuir* **2001**, *18*, 706–715.
58. Wertz, C. F.; Santore, M. M. Effect of Surface Hydrophobicity on Adsorption and Relaxation Kinetics of Albumin and Fibrinogen: Single-Species and Competitive Behavior. *Langmuir* **2001**, *17*, 3006–3016.
59. Wertz, C. F.; Santore, M. M. Adsorption and Relaxation Kinetics of Albumin and Fibrinogen on Hydrophobic Surfaces: Single-Species and Competitive Behavior. *Langmuir* **1999**, *15*, 8884–8894.